Miner Deposita (2006) 41: 68–81
DOI 10.1007/s00126-005-0041-7

ARTICLE

Jochen Kolb · Gregori A. Sakellaris · F. Michael Meyer

Controls on hydrothermal Fe oxide–Cu–Au–Co mineralization at the Guelb Moghrein deposit, Akjoujt area, Mauritania

Received: 3 June 2005 / Accepted: 30 November 2005 / Published online: 21 March 2006

Abstract The Guelb Moghrein Fe oxide–Cu–Au–Co deposit, with a total resource of 23.6 Mt at 1.88% Cu, 1.41 g/t Au, and 143 g/t Co, is hosted by an extensive metacarbonate body. However, it is restricted to up to 30-m wide tabular breccia zones developed parallel to discrete shear zones that transect the host metacarbonates. The Fe–Mg clinoamphibole–chlorite schists represent up to 1-m thick interlayer metasediments and localized viscous shearing in these shear zones. Siderite of the metacarbonate body was deformed into a breccia and was replaced by an ore and alteration assemblage comprised of Fe–Mg clinoamphibole, magnetite, pyrrhotite, chalcopyrite, graphite, Fe–Co–Ni arsenides, arsenopyrite, cobaltite, uraninite, and Bi–Au–Ag–Te minerals. In contact with wall rock amphibolites, the metacarbonate body is enveloped by an alteration halo up to 40 m wide, consisting of biotite, actinolite, grunerite, chlorite, calcite, albite, and quartz. The Guelb Moghrein ore body is structurally controlled by shear zones that developed in the footwall of a regional thrust zone. This thrust separates greenschist facies quartz–sericite schists and biotite–garnet–quartz schists of the Sainte Barbe volcanic unit in the hanging wall from amphibolite facies metavolcanic rocks, metacarbonates, and the Guelb Moghrein ore body of the Akjoujt metabasalt unit in the footwall. Peak temperatures of the latter unit are estimated by hornblende–plagioclase thermometry at 580±40°C. Thrusting was retrograde for the Akjoujt metabasalt unit, but prograde for the Sainte Barbe volcanic unit at P–T conditions of about 410±30°C and 2–3 kbar (garnet–biotite thermometry). Structural and petrological evidences suggest that the ore fluids migrated along the shear zones and reacted with the siderite in the metacarbonate. This evolution and the setting of Guelb Moghrein in the fold-and-thrust belt of the Pan-African to Variscan Mauritanides (Mauritania, West Africa) resemble Proterozoic Fe oxide–Cu–Au–Co deposits such as examples from the Tennant Creek and Mount Isa Inliers, Australia.

Keywords Fe oxide–Cu–Au–Co deposit · Guelb Moghrein · Akjoujt · Mauritania · Hydrothermal

Editorial handling: R. Moritz

Electronic Supplementary Material Supplementary material is available for this article at http://dx.doi.org/10.1007/s00126-005-0041-7

J. Kolb (✉) · G. A. Sakellaris · F. M. Meyer
Institute of Mineralogy and Economic Geology,
RWTH Aachen University,
52056 Aachen, Germany
e-mail: kolb@rwth-aachen.de

Introduction

Hydrothermal Fe oxide–Cu–Au–Co (IOCG) deposits share a number of distinguishing features: (1) an extensive alkali-rich alteration halo, (2) the presence of hydrothermal magnetite and/or hematite, (3) a structural control by a host-breccia, and (4) a common element association of Cu, Au, Co, Ni, As, LREE (Hitzman et al. 1992). Typical tectonic settings for IOCG deposits are (1) intracontinental terranes with anorogenic magmatism (e.g., Olympic Dam), (2) relatively young continental arc terranes with intermediate magmatism such as the Andes, and (3) fold-and-thrust belts (e.g., Tennant Creek and Mount Isa Inliers) (Hitzman 2000; Skirrow and Walsche 2002; Sillitoe 2003). Genetic models for IOCG deposits associated with magmatic events suggest that the major fluid and metal source lies in relatively primitive intrusives, which can be as deep as 10 km and, thus, may not be exposed (Porter 2002; Sillitoe 2003). The associated intrusive rocks are generally gabbroic to dioritic in composition, which may explain the Cu–Au–Co–Ni–As signature of the related ores. In contrast, IOCG deposits that are developed in fold-and-thrust belts are believed to have formed from basin fluids, metamorphic fluids, and/or highly saline basin brines derived from evaporites, which locally mix at the trap site (Porter 2002; Skirrow and Walsche 2002). This indicates

that no single genetic model can be developed for the IOCG deposits (Porter 2002; Sillitoe 2003).

In this paper, we present petrologic and structural data from the Guelb Moghrein deposit in northern Mauritania, which was recently classified as an IOCG type (Strickland and Martyn 2002). In particular, the geometry, kinematics, and mineralogy of the mineralized structures are described. Our data indicate ore formation in a compressive shear zone on the retrograde P–T path of a poorly known metamorphic host terrane in the northernmost Mauritanides.

Regional geology

The Akjoujt area, hosting the Guelb Moghrein deposit, lies on a bend of the Mauritanides chain, a complex, generally east-verging fold-and-thrust belt that extends from Senegal in the south to Western Sahara in the north (Fig. 1). It is generally regarded as a pile of allochthonous terranes thrusted toward the West African Craton in the east (Lécorché et al. 1989). About 30 km NE of Akjoujt, a thrust zone bounds the Mauritanides to the north and east to the Amsaga Basement, which comprises gneisses and granulites of the southwestern Archean Reguibat Shield and the Taoudéni Basin characterized by unmetamorphosed sedimentary rocks of Neoproterozoic to Devonian age. Muscovite K–Ar and Ar–Ar ages from this sole thrust indicate final thrusting of the Mauritanides at about 325–300 Ma, folding Devonian Molasse sedimentary rocks of the Taoudéni Basin (Lécorché and Clauer 1984; Dallmeyer and Lécorché 1989; Martyn and Strickland 2004). A series of overthrust sheets, which comprise basement schist and gneiss, defines the western edge in the Akjoujt area (Fig. 2). Thin marine Cretaceous to Quaternary sediments

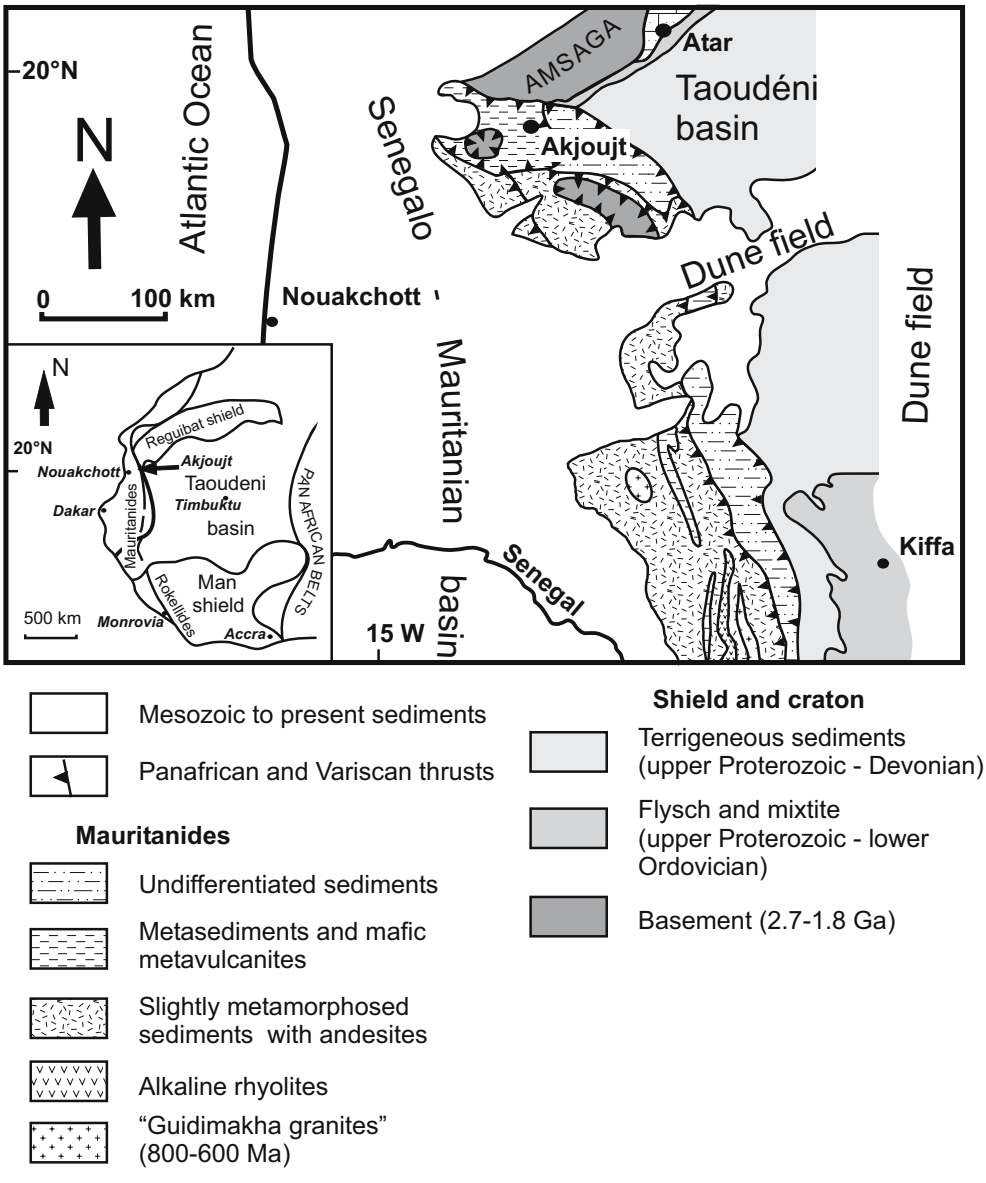

Fig. 1 Schematic geological map showing the Senegalo–Mauritanian basin and the various units of the Mauritanides, which were thrusted to the east onto the West African Craton. Akjoujt and the Guelb Moghrein deposit are situated in the northern part (modified after Le Page 1988; Lécorché et al. 1989)

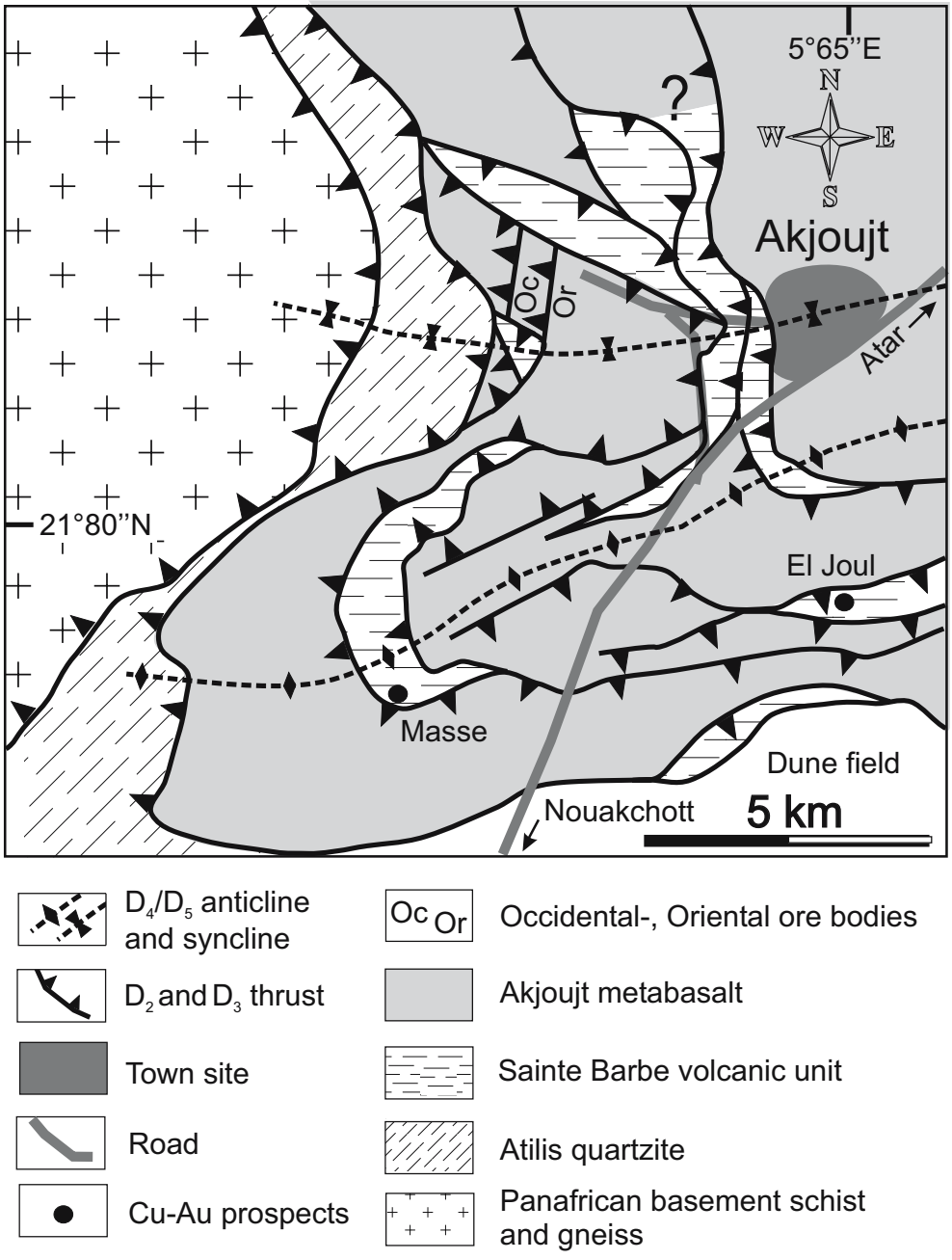

Fig. 2 Schematic geological map of the Akjoujt area (modified after Martyn and Strickland 2004). A complex set of D_2 and D_3 thrust faults outcrop to the west of the Akjoujt town site. The thrusts are folded with broadly E–W trending fold axes during D_4 and D_5. The Occidental (*Oc*) and Oriental (*Or*) ore bodies are located about 3 km to the west of the Akjoujt town center. Masse and El Joul represent local prospects for Cu and Au (Strickland and Martyn 2002)

obscure the western boundary of the Mauritanides for much of its length (Sougy 1969; Martyn and Strickland 2004).

Stratigraphy

The Akjoujt area features a supracrustal suite consisting of metamorphosed volcanic, volcaniclastic, and epiclastic rocks. The supracrustal stratigraphy is believed to consist of two groups, namely, the Eizzene Group and the Oumachoueïma Group, separated by an angular unconformity (Strickland and Martyn 2002; Martyn and Strickland 2004). The Eizzene Group, situated about 10 km to the NE of Akjoujt, is intruded by fine- to medium-grained granodiorite plutons, which are about 2 km in diameter. The basal Atilis quartzite of the Oumachoueïma Group unconformably overlies the plutons and the supracrustals of the Eizzene Group (Strickland and Martyn 2002; Martyn and Strickland 2004). These quartzites are overlain by mafic to intermediate lithologies of the Sainte Barbe volcanic unit, which is overlain by thick and extensive basalt flows with dolerite intrusives of the Akjoujt metabasalts (Strickland and Martyn 2002; Martyn and Strickland 2004). The age of the supracrustal rocks from the Akjoujt area is believed to be Upper Proterozoic, with very few arguments (Strickland and Martyn 2002; Martyn and Strickland 2004).

Tectonometamorphic evolution

The Akjoujt area is characterized by a complex set of folded and stacked thin skinned thrust sheets (Fig. 2). Five deformation events (D_1–D_5) are distinguished (Pouclet et al. 1987; Martyn and Strickland 2004). The D_1 deformation formed moderate folds and a weak regional S_1 foliation (Strickland and Martyn 2002; Martyn and Strickland 2004). During D_2, thrusting to the NNW created a layer-parallel S_2 foliation and recumbent folds. The peak metamorphic grade increases from lower to upper greenschist or lower amphibolite facies and rises stratigraphically upward toward the west. This suggests that the various lithological units were first metamorphosed and then inverted during subsequent eastward thrusting (Strickland and Martyn 2002).

The thrusting event might be linked to the Pan-African orogeny around 650–600 Ma (Dallmeyer and Lécorché 1989; Lécorché et al. 1989). This correlates well with the timing of collision and thrusting in the southern Mauritanides and Rokelides, Senegal (Ponsard et al. 1988) and in the Anti-Atlas, Western Sahara and Morocco (Inglis et al. 2004; Thomas et al. 2004). Ar–Ar ages of hornblende and muscovite record a cooling history of various terranes of the Mauritanides between ca 720–700, 683–670, and 595–570 Ma (Dallmeyer and Lécorché 1989).

ENE directed thrusting is attributed to D_3 and the formation of an S_3 foliation during retrograde greenschist facies conditions. This thrusting event is interpreted to be related to the late Pan-African orogeny, based on muscovite Ar–Ar cooling ages of ca 550–540 Ma and can possibly be correlated to the late-stage orogeny in the southern Mauritanides and Rokelides (Ponsard et al. 1988; Dallmeyer and Lécorché 1989). Gentle to moderate folds with ENE–WSW trending fold axes deformed the thrust sheets during D_4 and D_5, which is correlated with thrusting along the sole thrust during the Westphalian (Martyn and Strickland 2004).

Mine geology

The Guelb Moghrein deposit was exploited for copper in Neolithic times and the ancient workings were noted in 1931 by the French military. In 1967, the Société Minière de Mauritanie commenced the exploitation of the oxide ores of Guelb Moghrein, but the mine was closed in 1978 due to the increased fuel price and decrease in copper price. General Gold International SA made a joint venture agreement in 1994 and established the Guelb Moghrein Mines d'Akjoujt (GEMAK) SA in 1995 to conduct a feasibility study, which was completed in April 1997. Using a 1% Cu cutoff, the total resource has been calculated as 23.6 Mt at 1.88% Cu, 1.41 g/t Au and 143 g/t Co. From 1991 until 1996, about 45 kg gold was produced from the old mine tailings at 3.08 g/t Au (Strickland and Martyn 2002). In 2005, Guelb Moghrein will be reopened by a new company, of which 80% is owned by First Quantum Minerals and 20% by GEMAK.

The Guelb Moghrein ore bodies outcrop in two abrupt hills, namely, Occidental and Oriental, rising from the low undulating desert terrain on the western outskirts of Akjoujt town site. The main ore body is situated north of the east–west trending axis of a gentle synform, which folds an assemblage of multiple thrust sheets (Fig. 2). The wall rocks are dominated by amphibolites of the Akjoujt metabasalts and metacarbonate. Two Cu–Au prospects are located to the south and to the southwest of Akjoujt, respectively (Fig. 2; Strickland and Martyn 2002).

At Guelb Moghrein, ore bodies are hosted by two lensoid bodies of metacarbonate known as Occidental and Oriental (Fig. 2). The Oriental body is massive, about 250 m long and at least 150 m thick. Occidental is a broader, thinner, and longer lensoid body about 500 m across and up to 150 m thick, apparently tapering down-dip, but open to the depth. The metacarbonate is mainly composed of siderite and contains the bulk of the Fe oxide–Cu–Au–Co mineralization. Its origin is still a matter of discussion and is either explained by a sedimentary (Pouclet et al. 1987) or an alteration model, where the carbonate is formed by the alteration of amphibolite during the hydrothermal Fe oxide–Cu–Au–Co mineralization (Strickland and Martyn 2002). Copper- and gold-rich zones are interpreted to occur as multiple, coalescing lenses that are broadly elongated in the direction of discrete shear zones. Alteration and ore minerals are magnetite, Fe–Mg clinoamphibole, chalcopyrite, pyrrhotite, cubanite, arsenopyrite, cobaltite, pentlandite, graphite, valeriite, and gold (Strickland and Martyn 2002). The exsolution textures of chalcopyrite, pentlandite, cubanite, and pyrrhotite point to temperatures above 300–400°C for mineralization (Ramdohr 1957; Pouclet et al. 1987).

Weathering has produced an extensive oxidation zone characterized by goethite, siderite, hematite, with lesser amounts of anthophyllite, and graphite. Copper minerals include malachite, chalcopyrite, covellite, azurite, cuprite, native copper, and chrysocolla. Native gold is commonly attached to goethite and hematite (Strickland and Martyn 2002).

Lithostratigraphy and structure of Guelb Moghrein

Detailed open pit mapping revealed that the main lithologies at Guelb Moghrein are metasedimentary and metavolcanic rocks of the Sainte Barbe volcanic unit and metavolcanic rocks of the Akjoujt metabasalts as well as the metacarbonate body that contains the Fe oxide–Cu–Au–Co ore body.

The Sainte Barbe volcanic unit, comprising quartz–sericite schists and biotite–garnet–quartz schists, form the stratigraphic base. These rocks are thrusted onto the Akjoujt metabasalt unit along a broadly ESE–WNW trending shear zone in the south and southeast of the open pit (Fig. 3). ESE–WNW striking biotite–actinolite schists alternating with distinctly more massive and, thus, less deformed amphibolite lenses of the Akjoujt metabasalt unit underlie the central area (Fig. 3). A metacarbonate lens separates these lithologies into a northern and a southern part. In the eastern and western parts of the mining

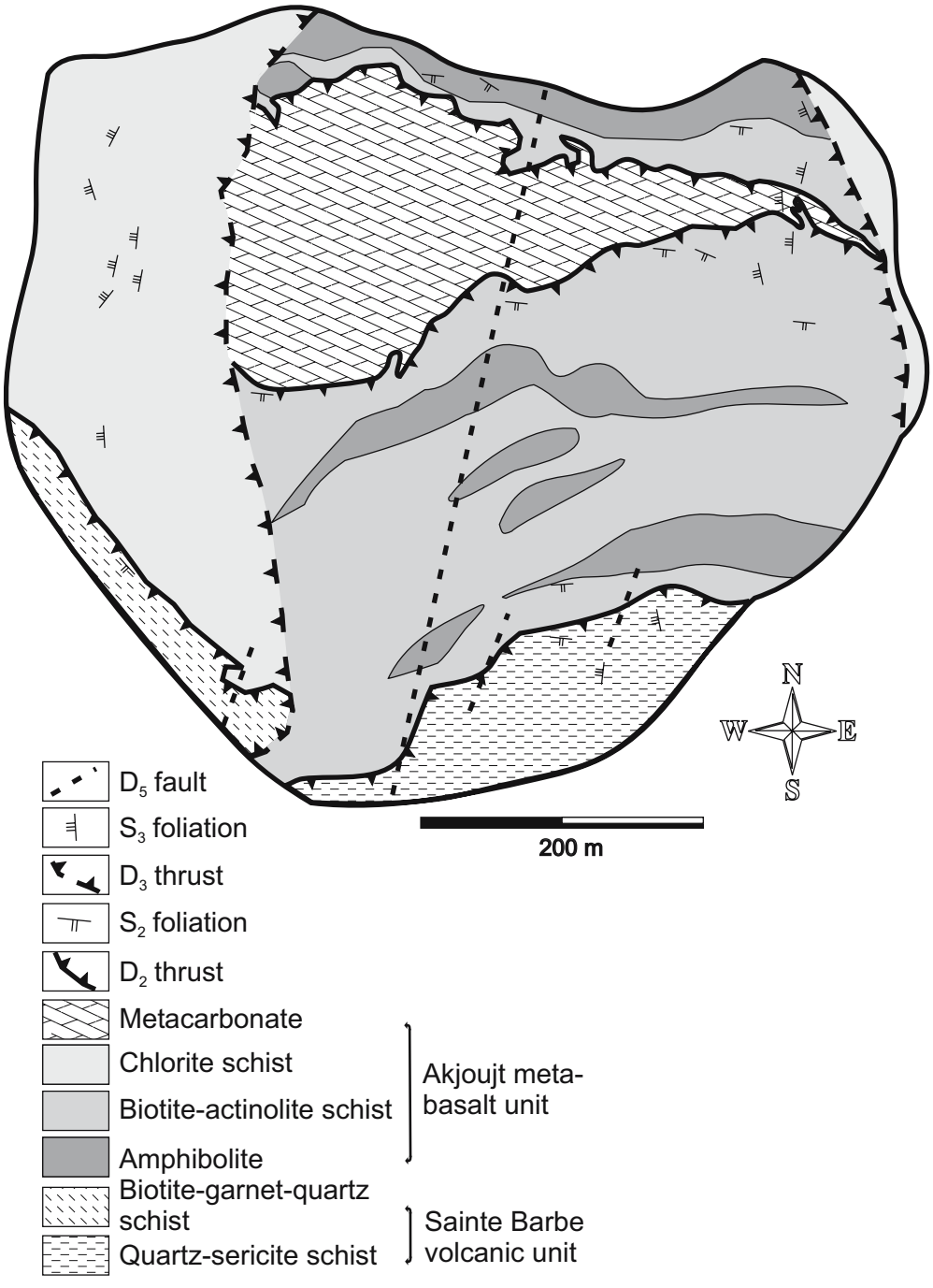

Fig. 3 Schematic geological map of the Guelb Moghrein open pit showing the major lithologies and structural features. The Fe oxide–Cu–Au–Co mineralization occurs in tabular bodies in the metacarbonate parallel to the ESE–WNW striking D_2 thrust zone

area, N–S trending chlorite schists that truncate all other ESE–WNW striking lithologies are exposed.

Sainte Barbe volcanic unit

The quartz–sericite schist is a light gray to greenish, well-foliated, fine-grained rock, comprising sericite, biotite, quartz, plagioclase, and chlorite (Fig. 4a). Quartz and plagioclase form porphyroclasts 0.4–1 mm in diameter and additionally occur in the fine-grained matrix. The rectangular to rounded quartz porphyroclasts enclose numerous micrometer-scale vitreous inclusions, implicating a magmatic origin for this rock type. Sericite, biotite, and chlorite define the closely spaced foliation (Fig. 4a), which is parallel to the tectonic contact of the Sainte Barbe volcanic unit and the Akjoujt metabasalt.

The biotite–garnet–quartz schist in the southwest of the pit is a yellowish brown, well-foliated, fine-grained rock comprising biotite, garnet, quartz, and chlorite (Fig. 4b). Biotite and chlorite define the closely spaced foliation. Garnet forms small (about 50 μm) porphyroclasts and porphyroblasts owing to their syn- to late-kinematic growth.

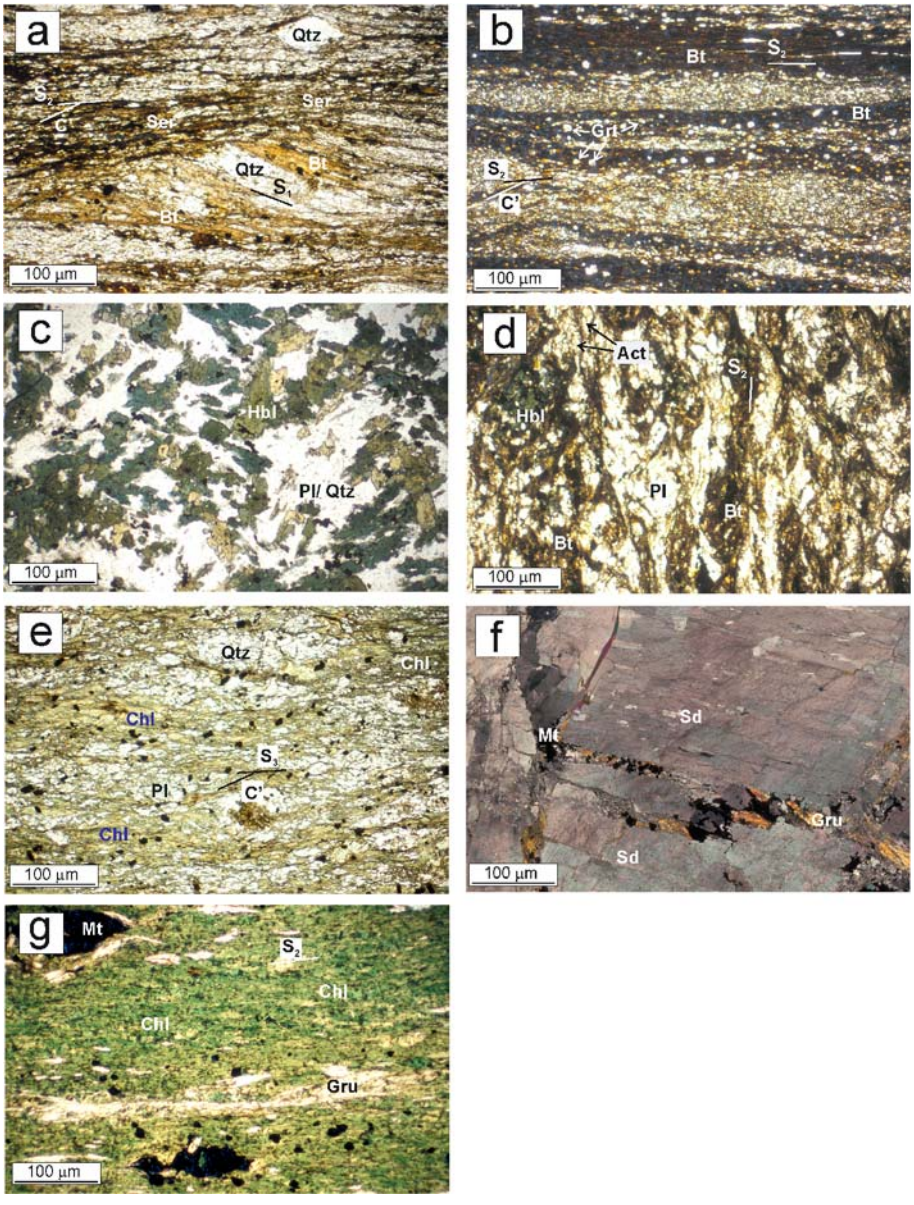

Fig. 4 Photomicrographs of the major wall rock lithologies. **a** Quartz–sericite schist with sericite (*Ser*) and biotite (*Bt*) defining the S_1, S_2 and C′ foliations and quartz (*Qtz*) porphyroclasts. **b** Biotite–garnet–quartz schist showing the peak metamorphic garnet (*Grt*), biotite assemblage. Garnet forms porphyroblasts and biotite is aligned parallel to the S_2 and C′ foliations. **c** Peak metamorphic hornblende (*Hbl*), plagioclase (*Pl*) paragenesis of the amphibolites showing no foliation. **d** Biotite–actinolite schist. Retrograde biotite and actinolite (*Act*) replace hornblende along the S_2 foliation. **e** In the chlorite schist, chlorite (*Chl*) replaced biotite and the amphiboles from the amphibolites along well-developed S_3 and C′ foliations. **f** Least-altered metacarbonate showing the large fractured and internally deformed siderite (*Sd*), with fracture-filling comprising grunerite (*Gru*) and magnetite (*Mt*). **g** The Fe–Mg clinoamphibole–chlorite schist is dominated by green chlorite parallel to the S_2 foliation and comprises minor magnetite and grunerite/cummingtonite

Akjoujt metabasalt unit

The amphibolite is a dark green massive, only slightly foliated rock, comprising amphibole, plagioclase, ilmenite, chlorite, sphene, and quartz (Fig. 4c). Euhedral plagioclase laths and interstitial amphibole form a well-preserved ophitic fabric. A fine-grained, plagioclase-rich amphibolite, which dominates in the eastern part of the open pit area, can be distinguished from a coarse-grained, amphibole-rich variety, which is mainly found in the western and southern pit area.

The biotite–actinolite schist is a fine-grained, green to dark brown rock comprising biotite, actinolite, albite, quartz, epidote, grunerite, chlorite, sphene, and relic hornblende and ilmenite (Fig. 4d). The moderately to closely spaced foliation is defined by biotite and actinolite. Biotite, actinolite, epidote, chlorite, and locally grunerite replace hornblende grains along their rims and cleavage planes. Plagioclase is recrystallized and locally forms bookshelf fabrics.

The chlorite schist has a closely spaced foliation defined mainly by alternating chlorite and quartz layers (Fig. 4e). Minor constituents are fine-grained sericite and disseminated grains of ilmenite and magnetite. Chlorite forms 20–100 µm long, light to yellowish green flakes. Quartz forms porphyroclasts (up to 300 µm) or elongated aggregates of fine grains (10 to 100 µm) with undulose extinction.

The metacarbonate is a massive, very coarse-grained, dark gray rock, which is mainly composed of euhedral to anhedral siderite up to 5 cm in diameter (Fig. 4f). Accessory phases include small, disseminated, needlelike magnetite inclusions. The contact with the biotite–actinolite schists of the Akjoujt metabasalt is always sharp and parallel to the broadly ESE–WNW trending foliation.

Locally along this contact and within the metacarbonate body, Fe–Mg clinoamphibole–chlorite schists occur as

narrow, up to 1 m wide stringers. These rocks are characterized by a closely spaced foliation and comprise about 90 vol.% chlorite and minor Fe–Mg clinoamphibole (mainly grunerite), magnetite, ilmenite, apatite, calcite, quartz, monazite, and allanite (Fig. 4g). It is, however, not clear whether this mineralogy represents, at least partly, the original composition of the precursor rocks or was formed during hydrothermal mineralization and alteration, because abundant minerals of the arsenide–sulfide–gold assemblage occur in this lithology.

Structural geology

Structural mapping in the open pit revealed two prominent structural features, i.e., an ESE–WNW trending and a N–S trending shear zone (Fig. 3). The shear zones are indicated by well-developed foliations and mylonitic fabrics in the various lithologies. Massive amphibolite and massive metacarbonate form lenses (lithons) parallel to the ESE–WNW trend.

In amphibolite, biotite–actinolite schist, and quartz–sericite schist a weak S_1 foliation is developed dipping moderately to the west. This S_1 foliation is defined by amphibole and biotite and can be observed in the lithons of an asymmetric S_1–S_2 crenulation cleavage.

The S_2 foliation is developed to various degrees in the different lithologies, but becomes more closely spaced in the biotite–actinolite schist and quartz–sericite schist in the direct vicinity of the ESE–WNW trending shear zones. The S_2 foliation dips moderately to the SSW/SW (Fig. 5a), with a well-developed down-dip L_2 mineral stretching lineation. The asymmetric crenulation cleavage, a S_2–C′ fabric (Fig. 4), and rotated porphyroclasts point to a reverse sense of movement along the shear zones during D_2.

Locally, the S_2 foliation is folded into upright, open F_3 folds with almost horizontal, N–S trending fold axes (Fig. 5b). In the NE area of the open pit, the S_2 foliation is transposed clockwise toward northerly trends and overprinted by a S_3 foliation, which is mainly defined by chlorite and best developed in the chlorite schist in the eastern and western pit area. The S_3 foliation dips moderately to the west (Fig. 5c) and shows a down-dip L_3 mineral stretching lineation. S_3–C′ fabrics (Fig. 4e) point to a reverse sense of movement during D_3.

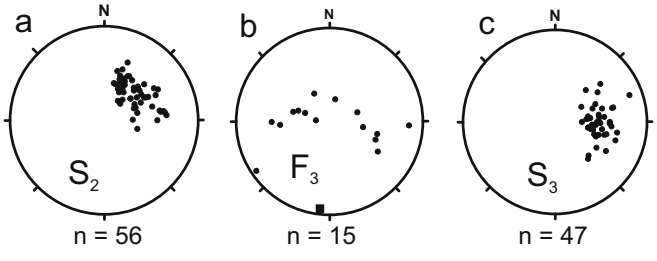

Fig. 5 Pole figures (equal area, lower hemisphere) of the major foliations collected from the open pit. **a** Poles to the S_2 foliation. **b** Poles to the S_2 foliation from a F_3 fold and calculated fold axis with shallow southerly plunge. **c** Poles to the S_3 foliation

In places, a conjugate set of S_4 foliations occurs that dips gently to moderately to the SW and that displays a normal sense of movement with only minor displacement during D_4. The latest stage of deformation is characterized by D_5 faults that trend N–S and have only minor displacement in the order of several meters (Fig. 3).

Structure of the Fe oxide–Cu–Au–Co mineralization

The Fe oxide–Cu–Au–Co mineralization is restricted to the lensoid metacarbonate body in the northern pit area (Fig. 3). It is situated (1) along the sheared hanging wall and footwall contacts and (2) in discrete shear zones truncating the metacarbonate parallel to the S_2 foliation. Copper-, Co-, and Au-rich zones occur in breccia zones developed in the metacarbonate and form multiple, up to 30 m wide, coalescing, foliation parallel lenses that dip moderately SW.

The mylonitic hanging wall and footwall contacts are represented by biotite–actinolite schists with increasing development of the S_2 foliation and alteration toward the contact with the metacarbonate, forming a ca 40–m wide alteration halo. The discrete shear zones truncating the metacarbonate are always associated with the Fe–Mg clinoamphibole–chlorite schists, which have a phyllonitic fabric (Fig. 4g). Individual shear zones are between 5 cm and 1 m wide and form an undulating, broadly tabular network subparallel to the S_2 foliation. A prominent S_2–C′ fabric together with a down-dip L_2 mineral stretching lineation points to a reverse sense of movement.

Two types of breccias are distinguished, which both are monomict:

1. Puzzlelike breccias, locally, form up to 5 cm wide and up to 20 cm long lenses parallel to S_2 in the Fe–Mg clinoamphibole–chlorite schists (Fig. 6a). The clasts are 50–200 μm in diameter and comprise angular fragments of chlorite and Fe–Mg clinoamphibole in a massive sulfide matrix. The puzzlelike fabric results from in situ fragmentation and displacement on a micrometer to millimeter scale. The angular fragments are not rotated and do not show any evidence of replacement.
2. A pebblelike breccia, consisting of siderite clasts within a matrix of a complex arsenide–sulfide–gold, magnetite, and Fe–Mg clinoamphibole assemblage, forms up to 30-m wide tabular bodies surrounding discrete D_2 shear zones in the metacarbonate body. The clast–matrix ratio and the fragment size increase systematically with the distance to the contact with biotite–actinolite and Fe–Mg clinoamphibole–chlorite schists. At the contact, massive sulfides contain <3% clasts and form a matrix-supported breccia (Fig. 6b). The siderite fragments are up to 1 cm in diameter and have a rounded to subrounded shape due to replacement by sulfides, magnetite, and Fe–Mg clinoamphibole at their rims, giving the breccia a pebblelike structure. Locally, the massive sulfide matrix is

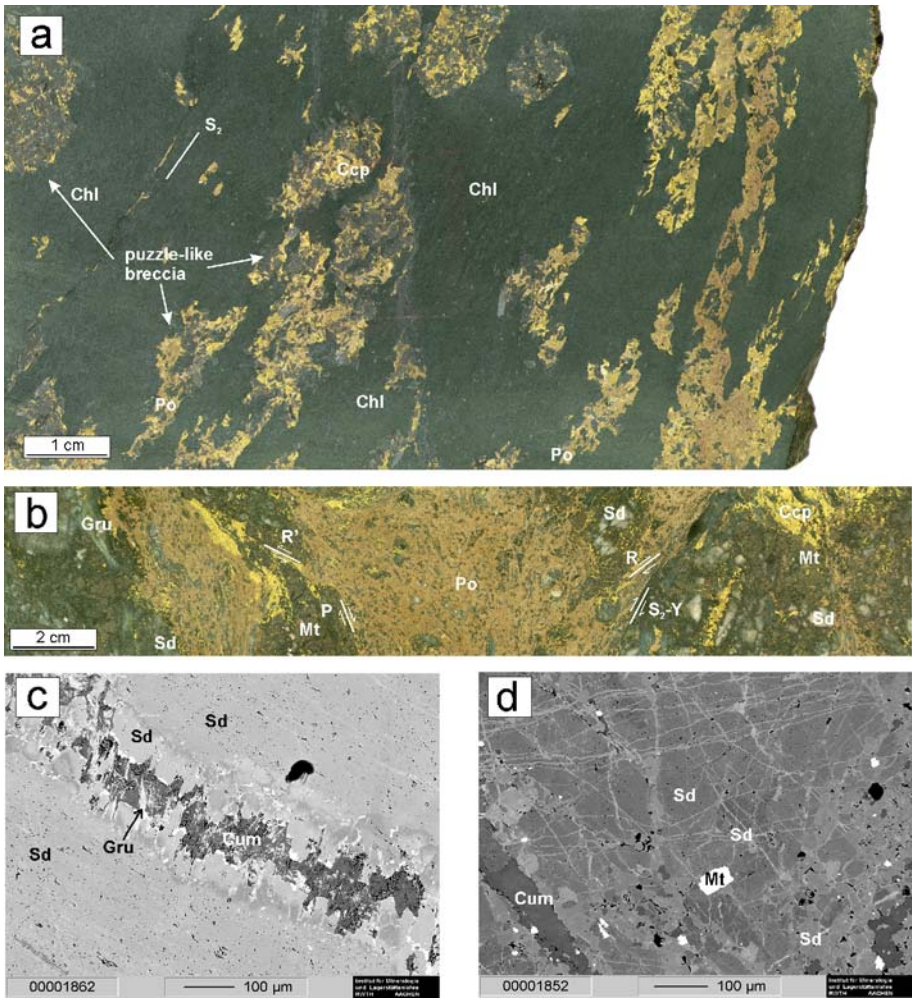

Fig. 6 **a** Photograph of a polished drill core from a mineralized Fe–Mg clinoamphibole–chlorite schist. Sulfides are dominated by pyrrhotite (*Po*) and chalcopyrite (*Ccp*), which form lensoid, puzzlelike breccias parallel to the S_2 foliation in a chlorite matrix. **b** Photograph of a polished drill core from a massive sulfide zone in brecciated siderite. Chalcopyrite and pyrrhotite, similarly, dominate the sulfide assemblage. Locally, magnetite, grunerite, and cummingtonite are developed as alteration minerals. Various types of Riedel shears are developed (R-, R′, P-, Y-shears). The Y-shears are parallel to the S_2 foliation. **c** Backscattered electron (BSE) image from a syntaxial vein developed in the distal breccia zone of the metacarbonate. Siderite with variable Fe–Mg ratio (*variable brightness*) and grunerite are grown from the walls into the fracture. The center of the fracture is filled by cummingtonite, suggesting hydrothermal Si metasomatism (*bright white zones* are charging effects). **d** BSE image from a least altered zone in the metacarbonate showing healed microfractures of variable orientation. Siderite in these healed microfractures is commonly more iron-rich than the original siderite of the metacarbonate, resulting in the brighter reflectance. Locally, siderite is recrystallized forming fine aggregates of similar composition as in the healed microfractures. A set of two microfracture orientations can be distinguished, which enclose an angle of about 70°, which suggests that the rhombohedral cleavage planes of the siderite crystallographically control initial fracture formation. Magnetite and cummingtonite occur preferably at microfracture intersections

truncated by pyrrhotite veinlets with a comb texture, which points to repeated fracturing during progressive brecciation of the metacarbonate.

In about 20 cm to 1 m distance to the lithologic contact with the biotite–actinolite and Fe–Mg clinoamphibole–chlorite schists, idiomorphic magnetite and Fe–Mg clinoamphibole predominate in the matrix. Here, the breccia has a clast-supported fabric with a network of variably oriented fractures of 100-µm to 3–cm width, suggesting in situ fragmentation of the original siderite. The fractures represent syntaxial veins filled with fibrous siderite and Fe–Mg clinoamphibole (Fig. 6c). In places, the vein-filling is brecciated suggesting multiple progressive episodes of fracturing. The orientation of fractures and fibers suggests development of various types of Riedel shears (R-, R′-, P-, and Y-shears; Fig. 6b), where the Y-shears are parallel to S_2. In the most distal parts, healed microfractures of variable orientation are found in the metacarbonate. These microfractures are visible in backscattered electron images or in traced fluid inclusion trails. The siderite in these healed microfractures is CL-bright (Fig. 6d), corresponding to a more iron-rich composition. Commonly, a set of two microfracture orientations can be distinguished, which enclose an angle of about 70°. This suggests that the rhombohedral cleavage planes of the siderite crystallographically control initial fracture formation.

Deposit structure

Former mining activities concentrated on the lensoid metacarbonate body, locally called Occidental, which dips to the SSW/SW parallel to the S_2 foliation. This metacarbonate body is disrupted by N–S trending D_3 shear zones in the western pit area resulting in a sharp contact with the N–S trending chlorite schist (Fig. 3). To the east, Oriental forms a large gossan body (Fig. 2), which suggests that D_3 shear zones displaced the Occidental and Oriental ore bodies and that both belong to the same stratigraphic horizon. The S_2 parallel, SSW/SW dipping lithological succession of the Akjoujt metabasalt including the metacarbonate and the overthrusted (D_2) Sainte Barbe volcanic unit is displaced by the N–S trending D_3 thrusts. In drill core, the Sainte Barbe volcanic unit is repeated at about a 130-m depth in bore holes of the eastern pit area. This indicates that D_3 shearing resulted in a displacement of at least 170 m along strike (Fig. 7).

Wall–rock alteration and ore mineralogy

The ca 40–m wide alteration halo developed in the Akjoujt metabasalt at the contact with the metacarbonate comprises biotite, actinolite, grunerite, chlorite, calcite, albite, and quartz (Fig. 8a). The bulk of the alteration assemblage occurs in the recrystallized feldspar matrix. In the distal alteration zone, hornblende is replaced by actinolite, grunerite, and biotite at grain boundaries, along cracks and cleavage planes. Locally, these minerals form pseudomorphs after hornblende, replacing the original minerals parallel to the S_2 foliation. Modal proportions of biotite, chlorite, and grunerite decrease gradually away from the contact between the metacarbonate and the biotite–actinolite schist. Notably, the alteration halo lacks any sulfide ore minerals. Predominantly in the eastern area of the open pit, the alteration assemblage of grunerite, biotite, and calcite forms lensoid lithons enveloped by the S_3 foliation, indicating that D_3 deformation postdated hydrothermal alteration and mineralization.

Locally, small lenses of plagioclase-rich amphibolites occur in the Akjoujt metabasalts, which are characterized by a typical biotite, albite, quartz, muscovite, tourmaline, and andalusite alteration paragenesis (Fig. 8b).

The Fe–Mg clinoamphibole–chlorite schists within the metacarbonate body comprise chlorite, Fe–Mg clinoamphibole, magnetite and accessory apatite, and monazite, which might partly belong to a primary mineral assemblage

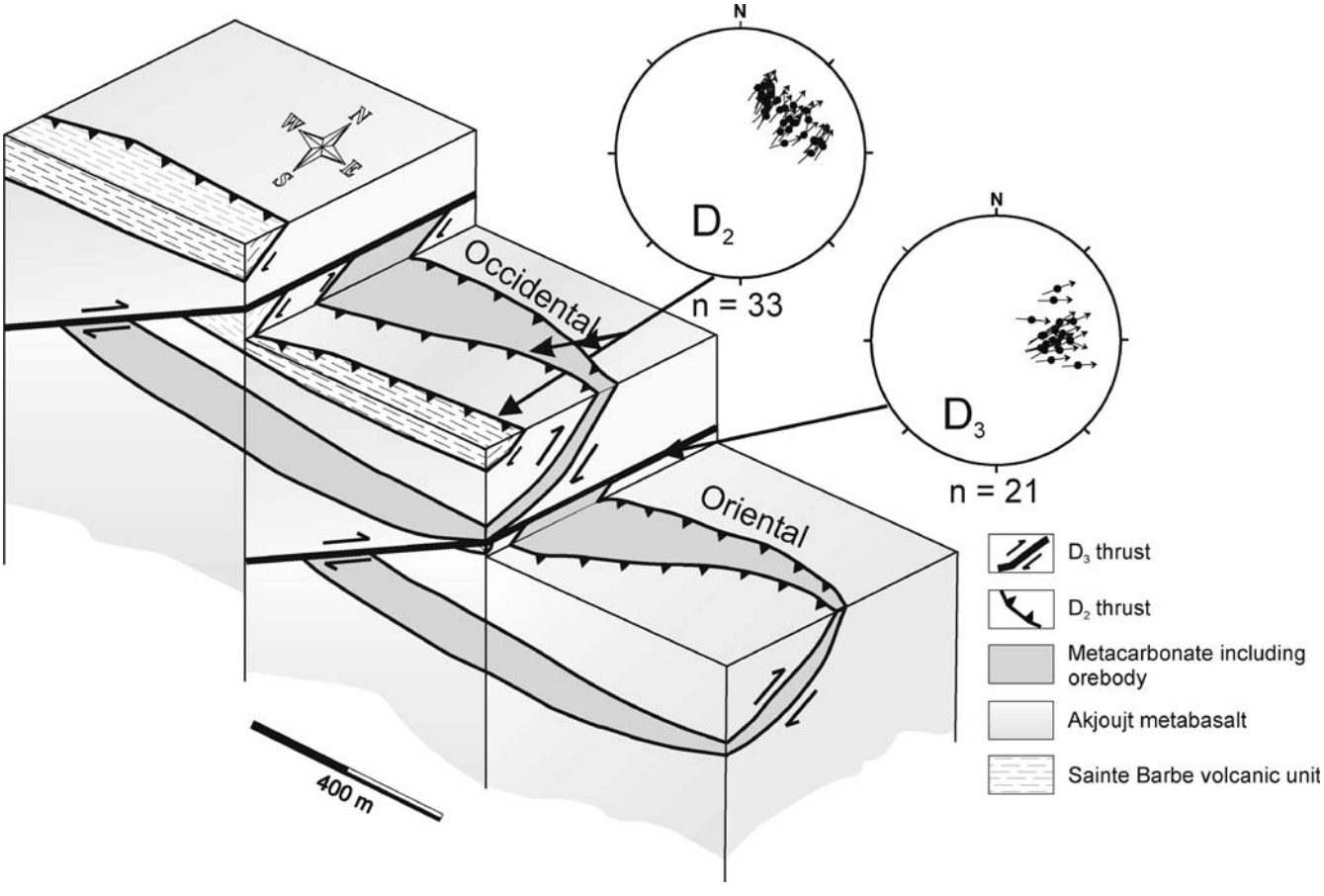

Fig. 7 Schematic block diagram showing the relationships of D_2 and D_3 structures and the resulting geometry of the Guelb Moghrein ore body. The *central block* corresponds to the location of the open pit. The vertical displacement between the Occidental ore body and the Oriental ore body is at least 130 m. Additionally, in the Hoeppener diagrams (equal area, lower hemisphere) of the S_2 and S_3 foliations, the related mineral stretching lineations and shear sense are given

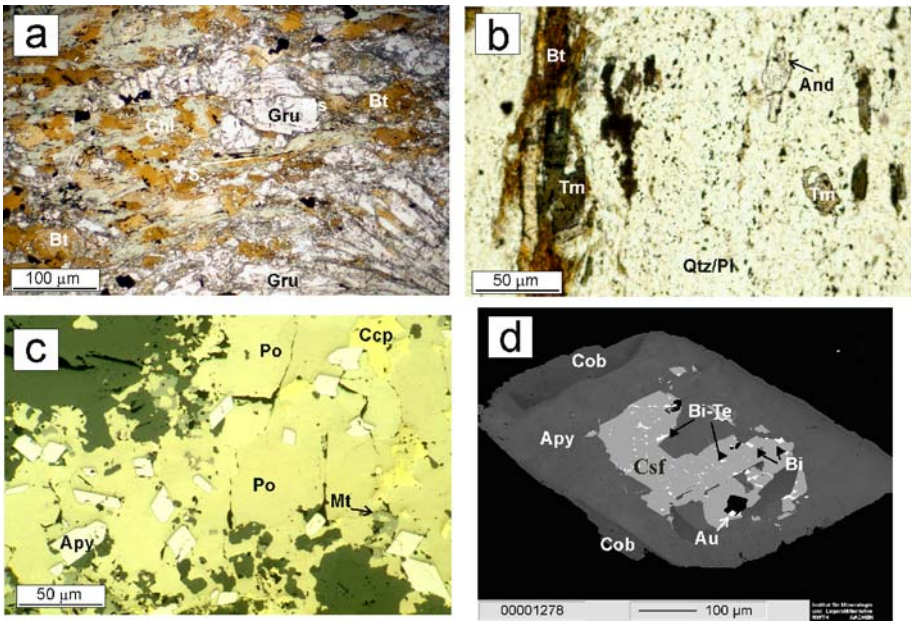

Fig. 8 **a** Photomicrograph of the characteristic grunerite–biotite–chlorite alteration assemblage in the biotite–actinolite schist proximal to the contact with the metacarbonate. **b** Photomicrograph showing the alteration assemblage of biotite, tourmaline (*Tm*) and andalusite (*And*) in plagioclase-rich amphibolites. **c** Photograph of a polished section with the main ore minerals, i.e., pyrrhotite, chalcopyrite, arsenopyrite (*Apy*), and magnetite in the massive sulfide zones. **d** BSE image of the composite grains with clinosafflorite (*Csf*) rimmed by arsenopyrite and cobaltite (*Cob*). Gold (*Au*), bismuth (*Bi*), and Bi-tellurides (*Bi–Te*) form inclusions in the clinosafflorite

(see above). The matrix of the small, puzzlelike breccia zones mainly comprises pyrrhotite and chalcopyrite (Fig. 6a).

Similarly, pyrrhotite and chalcopyrite are the dominant ore minerals in the matrix of the larger breccia zones, which are developed in the metacarbonate (Figs. 6b and 8c). Pyrrhotite typically forms anhedral aggregates and is variably deformed displaying exsolution lamellae (30–50 µm) of troilite and pentlandite. Chalcopyrite occurs also as anhedral aggregates cementing the fractures of the breccia in addition to small inclusions in pyrrhotite. Locally, cubanite forms exsolution lamellae in chalcopyrite grains. This major sulfide assemblage replaces the siderite clasts along grain boundaries, cleavage planes, and fractures.

Minor constituents are magnetite, graphite, Fe–Co–Ni arsenides, arsenopyrite, cobaltite, uraninite, and Bi–Au–Ag–Te minerals. The Fe–Co–Ni arsenides, arsenopyrite, and cobaltite (CoAsS) form medium to coarse (up to 3 mm), euhedral composite and strongly zoned grains (Fig. 8d). The cores are commonly formed by anhedral clinosafflorite ($CoAs_2$). At the outer rims, locally flame- or bleblike, 10–30 µm nickeline (NiAs) grains are developed. The clinosafflorite grains are rimmed by zoned arsenopyrite (Fig. 8d). The rims of these composite grains are locally made up of cobaltite, which also occurs as individual, idiomorphic grains between 0.5 and 3 mm in diameter. Abundant minute grains (maximum of 20 µm) of native gold, electrum, native bismuth, maldonite, Bi–tellurides, and rarely Ag–Au–tellurides form inclusions in clinosafflorite. The Bi–tellurides comprise hedleyite (Bi_7Te_3) and pilsenite (Bi_4Te_3). The identified minerals representative of the Ag–Au–tellurides are stuetzite ($Ag_{5-x}Te_3$) and petzite ($AuAg_3Te_2$).

The abundance of magnetite and Fe–Mg clinoamphibole increases with increasing clast–matrix ratio in the breccia. The syntaxial veins are typically composed of zoned siderite with variable Fe–Mg ratios together with grunerite at the vein walls (Fig. 6c). Cummingtonite and magnetite fill the center of the veins.

Metamorphism

Three metamorphic mineral assemblages are distinguished in the amphibolites. They are characterized by a peak metamorphic ferropargasite–albite paragenesis, which is replaced by an actinolite–epidote–albite paragenesis (biotite–actinolite schist) and subsequently by a chlorite–quartz paragenesis (chlorite schist). This suggests a retrograde evolution from peak metamorphic amphibolite facies to lower greenschist facies conditions. Amphibolite facies peak conditions are also suggested by the siderite–magnetite assemblage in the metacarbonate, which probably formed by decomposition of siderite at temperatures >500°C (Ellis and Hiroi 1997). The fact that actinolite is aligned parallel to the S_2 foliation and chlorite is parallel to the S_3 foliation indicates that the D_2 reverse shearing was associated with retrogression in the upper greenschist facies and that the D_3 reverse shearing occurred during lower greenschist facies conditions. During D_4, chlorite formed on the S_4 foliation in the lower greenschist facies.

In contrast, the mineral assemblages in the quartz–sericite schist and the biotite–garnet–quartz schist are typical of the upper greenschist facies. The well-preserved quartz porphyroclasts with vitreous inclusions in the quartz–sericite schist again indicate that peak metamorphism did not exceed upper greenschist facies conditions to any extend. A retrograde chlorite–quartz assemblage is also developed in these lithologies parallel to the S_3 foliation, which points to lower greenschist facies conditions during the D_3 deformation event.

To constrain the metamorphic conditions, two different geothermometers were applied to mineral assemblages of

the wall rocks. The mineral compositions of amphibole, plagioclase, garnet, and biotite were determined by a JEOL JXA-8900R electron microprobe on polished thin sections. Operating conditions were 15 kV and 2 mA with a defocused beam 10 μm in diameter. The analytical data are given in tables in the electronic supplementary material (ESM).

P–T conditions of peak metamorphism

The amphiboles in the amphibolite have a limited compositional variation, ranging from ferropargasite to ferroan pargasitic hornblende and ferrotschermackite to ferrohornblende from core to rim, depending on slight variations in their alkali contents. In amphibolites with higher Mg number, amphiboles range in composition from magnesio-hornblende in the core to actinolitic hornblende at the rim. The actinolitic hornblende rims are interpreted to have formed during retrograde metamorphism in the upper greenschist facies. Plagioclase is albite with anorthite contents ranging between $An_{0.7}$ and $An_{5.4}$. Albite is in textural equilibrium with the hornblende.

Peak metamorphic temperatures were calculated to 580±40°C at 5 kbar (Table 1) by the method after Holland and Blundy (1994), using the calibration for the reaction edenite + 4 quartz ↔ tremolite + albite. A pressure of 5 kbar is believed to be a reasonable pressure estimation for the regional metamorphic terrane. The low anorthite-content of plagioclase is unusual for the calculated temperature conditions and can possibly be explained by seafloor alteration of the amphibolite precursor rocks before metamorphism, which is also hinted by the high Mg number of some amphibolites. The calculated temperature, therefore, has to be taken with care as it possibly represents a minimum estimate of metamorphic peak conditions. They are, however, consistent with observed mineral fabrics and parageneses described above.

P–T conditions of retrograde metamorphism during D_2

Line traverses of larger garnet in the biotite–garnet–quartz schist display simple, bell-shaped, prograde zoning profiles, with increased almandine (50–62%) and decrease in spessartine (20–7%) contents at the rims. The grossular content varies in a small range between 21 and 26%. In contrast, most of the smaller garnets (Fig. 4b) have a nearly constant composition similar to the rim composition of the zoned garnets. Biotite is of a uniform composition with the Fe/Fe+Mg ratio varying between 0.64 and 0.72. Representative garnet and biotite analyses were chosen for the application of garnet–biotite thermometry. For the temperature calculation, calibrations were used, which take into account the Fe–Mg–Ca–Mn and Al–Ti solid solutions in garnet (Hodges and Spear 1982; Pertchuk and Lavrenteva 1983; Dasgupta et al. 1991; Bhattacharya et al. 1992). The average calculated temperature from all four calibrations is 410±30°C at 3 kbar (Table 2). The calibration from Holdaway (2000) was not applied because it consistently yielded unrealistically high temperatures.

The calculated temperature of 410±30°C is consistent with the retrograde, greenschist facies paragenesis of actinolite–epidote–albite in the amphibolite. This, together with the prograde garnet zoning in the garnet–biotite–quartz schist, suggests that D_2 thrusting of the Sainte Barbe volcanic unit onto the Akjoujt metabasalt occurred during upper greenschist facies conditions, where the Sainte Barbe volcanic unit is on the prograde path, whereas the Akjoujt metabasalt is already retrograde.

P–T conditions of mineralization

The biotite–actinolite–grunerite–chlorite alteration paragenesis in the biotite–actinolite schist is developed parallel to the S_2 foliation, which points to a formation during D_2 thrusting under upper greenschist facies conditions at 410±30°C. The presence of andalusite as alteration mineral in the plagioclase-rich amphibolites indicates that the pressure during this metamorphic stage did not exceed 2–3 kbar.

Similar P–T conditions are needed to stabilize the grunerite–chlorite paragenesis in the metacarbonate and Fe–Mg clinoamphibole–chlorite schist (Fig. 6a), which has a stability field between 310 and 430°C at 4 kbar, which becomes even smaller at lower pressures (Miyano and Klein 1989). At temperatures of about 400°C, grunerite forms according to the reaction 7 siderite + 8 quartz + H_2O ↔ grunerite + 7 CO_2 at a pressure as low as 2 kbar under considerable high XCO_2 conditions, which can be expected to have prevailed in the metacarbonate rock (Miyano and Klein 1989). The arsenide–sulfide–gold assemblage and the exsolution textures in chalcopyrite and pyrrhotite point to temperatures at about 400°C for mineralization and exsolution during re-equilibration during retrogression (Ramdohr 1957). Based on this line of evidence, P–T conditions of 410±30°C and 2–3 kbar are proposed for the Fe oxide–Cu–Au–Co mineralization at Guelb Moghrein.

Table 1 Calculated temperatures for the amphibole-plagioclase pairs, by the method of Holland and Blundy (1994)

T-S No.	26016	26016	26028	26029	26037	26037	26047	26047	26047	26042	26028	26016
Calculated temperature [°C]	532	533	563	555	594	540	614	612	642	618	576	567
Average temperature [°C]	580±40°C											

Note: Temperatures are calculated for a pressure of 5 kbar. Compositional data see ESM

Table 2 Garnet-biotite thermometry calculated after four selected calibrations

Grt-Bt pair	B92-HW[1]	Dasg91[2]	HS82[3]	PL83[4]
1	375	378	396	410
2	389	371	417	427
3	426	459	477	461
4	395	370	426	430
5	389	373	411	419
6	394	339	408	421
7	422	391	446	438
8	434	410	471	458
9	406	361	419	424
10	403	365	409	416
11	379	369	414	420
12	382	370	419	417
13	374	379	424	426
mean	397	380	426	428
1σ	20	29	24	15

Notes [1]Bhattacharrya et al. (1992); [2]Dasgupta et al. (1991); [3]Hodges and Spear (1982); [4]Pertchuk and Lavrenteva (1983)

Discussion

The moderately SSW/SW dipping metacarbonate body exerts a strong lithological control on the Cu–Au–Co mineralization of the Guelb Moghrein deposit. The mineralization is developed parallel to the D_2 shear zones, which has previously led to the interpretation that the carbonate represents an intense alteration halo formed by hydrothermal alteration of sheared amphibolite (Strickland and Martyn 2002). However, several points argue against the hypothesis that siderite and the mineralization formed contemporaneously:

1. Siderite from the metacarbonate body is itself replaced by Fe–Mg clinoamphibole, magnetite, and the arsenide–sulfide–gold assemblage.
2. Siderite is deformed, forming the clasts in a breccia with a matrix composed of the typical alteration and ore mineral assemblage.
3. The contact between amphibolites and the metacarbonate is always sharp and no amphibolite relics are found in the metacarbonate.

The Fe–Mg clinoamphibole–chlorite schists, comprising of minerals such as apatite, monazite, and allanite, are also unlikely to represent alteration products of amphibolite. Instead, we interpret the metacarbonate to represent a marine sediment, in accordance with earlier works on Guelb Moghrein (Ba Gatta 1982; Pouclet et al. 1987). Many banded iron formations containing siderite are known from the area around Akjoujt (Martyn and Strickland 2004). We suggest, therefore, that the siderite formed as ironstone on a continental shelf and the Fe–Mg clinoamphibole–chlorite schists represent metamorphosed and altered iron-rich interlayer sediments with terrigeneous input.

Structural control of hydrothermal alteration

A structural control of the Cu–Au–Co mineralization is provided by the D_2 shear zones, which reactivated the lithological contact between metacarbonate, amphibolite, and Fe–Mg clinoamphibole–chlorite schists in the footwall of the D_2 thrust, separating the Akjoujt metabasalt from the Sainte Barbe volcanic unit. Retrograde D_2 shearing of amphibolite in the upper greenschist facies resulted in the formation of biotite–actinolite schists. The rheologically weak Fe–Mg clinoamphibole–chlorite schists localized viscous shearing in the metacarbonate body and controlled the brittle deformation of siderite and, therefore, mineralization and alteration in the metacarbonate (cf.; Figs. 4g, 6a,b).

D_2 shearing was partitioned into ductile deformation of the biotite–actinolite and Fe–Mg clinoamphibole–chlorite schists and brittle deformation of the metacarbonate. In the biotite–actinolite schist, fabric development and degree of biotite–chlorite–grunerite–calcite alteration increase toward the metacarbonate contact. Therefore, the development of porosities for hydrothermal fluid flow is strongly related to ductile strain, mainly accommodated by crystal-plastic deformation of biotite, chlorite, and plagioclase (Fig. 4d). The pervasive style of alteration suggests that a grain-scale, meshlike porosity system was developed during D_2 shearing. However, this alteration zone is not mineralized.

The economic mineralization is hosted by the brecciated metacarbonate enveloping the Fe–Mg clinoamphibole–chlorite schists. The geometry of this system resembles the distribution of fault gouge and damage zones in brittle faults at lower temperatures (Caine et al. 1996; Evans et al. 1997). The Fe–Mg clinoamphibole–chlorite schist is deformed by viscous deformation of chlorite and to a lesser extent of grunerite. It contains small lenses of puzzlelike, sulfide-filled breccia, which are interpreted as hydraulic breccias. Such breccias require a supralithostatic fluid pressure for their formation. Consequently, the Fe–Mg clinoamphibole–chlorite schist is considered to have a relatively reduced permeability similar to fault gouge zones in brittle faults.

Siderite is rheologically stronger at temperatures of about 400°C and, therefore, deformation results in the formation of breccias that are symmetrically developed in the hanging wall and in the footwall of the schists. The breccias evolve progressively from massive sulfide breccias to crystallographically controlled microfractures in zones 5 to 30 m away from the lithological contact. Overprinting relationships of various vein generations in the massive breccias indicate repeated episodes of fracture formation. Similar to the damage zones in brittle faults, these breccia zones account for the bulk permeability of the D_2 shear zones at Guelb Moghrein, hence, host the economic Fe oxide–Cu–Au–Co mineralization. Mineralogic fabrics such as grunerite rosettes and idiomorphic crystal surfaces in veins suggest growth of these crystals in open or fluid-filled space, proving large porosity systems in the breccia zones. The rheological contrast between siderite in the metacar-

bonate and the Fe–Mg clinoamphibole–chlorite schist at upper greenschist facies conditions is the key factor for the structural control of hydrothermal mineralization.

Hydrothermal mineralization at Guelb Moghrein and the IOCG class of deposits

The Guelb Moghrein deposit has several features in common with the IOCG class of deposits, such as: (1) a characteristic metal association of Fe–Cu–Au–Co–Ni–As–U–LREE, as indicated by the ore mineral paragenesis; (2) a dominance of magnetite as Fe oxide mineral; (3) a dominance of low-sulfur ore minerals such as pyrrhotite, pentlandite, arsenopyrite, and cobaltite; and (4) a lack of quartz veins. However, in contrast to many IOCG deposits, the alteration halo at Guelb Moghrein is very narrow (about 40 m). The hydrothermal mineralization is closely related to D_2 deformation under retrograde metamorphic conditions in the upper greenschist facies. Regionally, the deposit is hosted by a metamorphic terrane, which is characterized by a complex arrangement of thrust faults and folds characteristic of a fold-and-thrust belt (Martyn and Strickland 2004). This geological setting closely resembles the setting of IOCG deposits in Australia, such as the Ernest Henry and Starra deposits, and those of the Tennant Creek Inlier (Rotherham 1997; Mark et al. 2000; Skirrow and Walsche 2002). The P–T conditions of 410±30°C and 2–3 kbar for mineralization at Guelb Moghrein are similar to those reported for Ernest Henry (Mark et al. 2000). In these deposits, the hydrothermal fluid flow is strongly structurally controlled by thrust fault systems, focusing basin brines or metamorphic fluids to the trap site (Skirrow and Walsche 2002). Although the fluid source is currently not known for the hydrothermal mineralization at Guelb Moghrein, the structural control of the mineralization by a D_2 thrust suggests a regional fluid migration pattern in the complex thrust system in the Akjoujt area. The Australian deposits also have a strong lithological control by hydrothermal ironstones, which formed earlier than the Au–Cu–Bi mineralization (Skirrow and Walsche 2002). The highly reactive ironstones are the favorable trap sites for the hydrothermal mineralization. A similar situation is suggested for the Guelb Moghrein deposit, where the siderite of the metacarbonate represents the reactant mineral for the hydrothermal, Cu–Au–Co bearing fluids. Further exploration for IOCG deposits in the Mauritanides should, therefore, focus on thrust zones, which are in direct neighborhood with siderite bearing metacarbonate horizons and possibly also banded iron formations, which are regionally widespread, rheologically strong, and reactive. The key feature of the IOCG mineralization at Guelb Moghrein is the combination of a highly permeable fluid pathway along a shear zone and a highly reactive lithology.

Conclusions

In this paper, we provide data about the geometry, kinematic history, alteration, and mineralization of the Guelb Moghrein Fe oxide–Cu–Au–Co deposit. The structural and petrographic data strongly suggest that the hydrothermal mineralization was emplaced in a shear zone system during regional D_2 thrust tectonics in brecciated metacarbonate that acted as a rheologically and chemically favorable lithology. The following key points emphasize this:

1. The economic Fe oxide–Cu–Au–Co mineralization occurs in up to 30-m wide tabular bodies parallel to discrete D_2 shear zones. These shear zones have a characteristic geometry of central, ductile Fe–Mg clinoamphibole–chlorite schist surrounded by a progressively developed breccia of fractured siderite. In these damage zones, a massive sulfide–arsenide–gold assemblage formed together with magnetite and Fe–Mg clinoamphibole in more distal parts.
2. Retrograde shearing during hydrothermal mineralization in the footwall of the regional D_2 thrust was contemporaneous with nappe tectonics during prograde metamorphism at 410±30°C and 2–3 kbar in the hanging wall lithologies. These P–T conditions are consistent with the alteration and ore mineral parageneses. They, however, formed in lithologies, which are already on the retrograde P–T path.
3. Shearing under upper greenschist facies conditions resulted in strain partitioning into brittle deformation of siderite from the metacarbonate and viscous deformation of Fe–Mg clinoamphibole–chlorite schists. This formed a highly permeable damage zone in the metacarbonate, which hosts the economic mineralization.
4. Siderite of the metacarbonate is replaced by magnetite, Fe–Mg clinoamphibole, and the arsenide–sulfide–gold assemblage, which strongly suggests that the hydrothermal ore fluid reacted with the host rocks forming the Fe oxide–Cu–Au–Co deposit.
5. Subsequent D_3 thrusting and folding in the lower greenschist facies displaced the mineralized structures at various scales, which resulted in the separation of the Occidental and Oriental ore bodies by at least 170 m. No remobilization of ore minerals is associated with these events.

Although the exact age of D_2 thrusting and mineralization is not known, the overprinting relationships of D_3–D_5 events, which are related to the Pan-African and Variscan orogeny, respectively, suggest that hydrothermal IOCG mineralization at Guelb Moghrein is contemporaneous with regional D_2 thrusting in either a Pan-African or earlier fold-and-thrust belt.

Acknowledgements The authors would like to thank Mohamed El Moctar O. M. El Hacen (Deputy General Manager, GEMAK, Nouakchott) and Aboubekrine O. A. dit Ebaye (Director MORAK, Akjoujt) for their support in Mauritania and the permission to publish the results of this study. Dr. Karsten Eden is thanked for fruitful discussions about the deposit from which this manuscript greatly benefited. A. Dziggel is thanked for comments on an earlier version of this manuscript. Thorough reviews from Y. Watanabe and M. Jébrak helped greatly to improve the manuscript. This study was made possible through grant Me 1425/6-1/2 of the Deutsche Forschungsgemeinschaft.

References

Ba Gatta A (1982) Contribution à l'étude géologique et minéralogique du gisement d'Akjoujt, Mauritanie. PhD Thesis, Université Orléans, Orléans

Bhattacharya A, Mohanty L, Maji A, Sen SK, Raith M (1992) Non-ideal mixing in the phlogopite-annite binary: constraints from experimental data on Fe–Mg partitioning and a reformulation of the biotite–garnet geothermometer. Contrib Mineral Petrol 11:87–93

Caine J, Evans JP, Forster CB (1996) Fault zone architecture and permeability structure. Geology 26:1025–1028

Dallmeyer RD, Lécorché JP (1989) $^{40}Ar/^{39}Ar$ polyorogenic mineral age record within the central Mauritanide orogen, West Africa. Geol Soc Amer Bull 101:55–70

Dasgupta S, Sengupta P, Guha D, Fukuoka M (1991) A refined garnet–biotite Fe–Mg exchange geothermometer and its application in amphibolites and granulites. Contrib Mineral Petrol 109:130–137

Deer WA, Howie RA, Zussman J (1992) An introduction to rock-forming minerals, 2nd edn. Longman Group, Harlow, UK, p 696

Droop GTR (1987) A general equation for estimating Fe^{3+} concentrations in ferromagnesian silicates and oxides from microprobe analyses, using stoichiometric criteria. Mineral Mag 51:431–435

Ellis DJ, Hiroi Y (1997) Secondary siderite–oxide–sulphide and carbonate–andalusite assemblages in cordierite granulites from Sri Lanka: post-granulite facies fluid evolution during uplift. Contrib Mineral Petrol 127:315–335

Evans JP, Forster CB, Goddard JV (1997) Permeability of fault-related rocks, and implications for hydraulic structure of fault zones. J Struct Geol 19:1393–1404

Hitzman MW, Oreskes N, Einaudi MT (1992) Geological characteristics and tectonic setting of Proterozoic iron oxide (Cu–U–Au–REE) deposits. Precambrian Res 58:241–287

Hitzman MW (2000) Iron oxide–Cu–Au deposits: what, where, when and why. In: Porter TM (ed) Hydrothermal iron oxide copper–gold & related deposits: a global perspective. Australian Mineral Foundation, Adelaide, pp 9–25

Hodges KV, Spear FS (1982) Geothermometry, geobarometry and the Al_2SiO_5 triple point at Mt. Moosilauke, New Hampshire. Am Mineral 67:1118–1134

Holdaway MJ (2000) Application of new experimental and garnet Margules data to the garnet–biotite geothermometer. Am Mineral 85:881–892

Holland TJB, Blundy J (1994) Non-ideal interactions in calcic amphiboles and their bearing on amphibole–plagioclase thermometry. Contrib Mineral Petrol 116:433–447

Inglis JD, MacLean JS, Samson SD, D'Lemos RS, Admou H, Hefferan K (2004) A precise U–Pb zircon age for the Bleïda granodiorite, Anti-Atlas, Morocco: implications for the timing of deformation and terrane assembly in the eastern Anti-Atlas. J Afr Earth Sci 39:277–283

Le Page A (1988) Rock deformation associated with the displacement of allochthonous units in the central segment of the Caledono–Hercynian Mauritanide belt (Islamic Republic of Mauritania and eastern Senegal). J Afr Earth Sci 7:265–283

Lécorché JP, Clauer N (1984) First radiometric date (K/Ar) on the front of the Mauritanides in the Akjoujt region (Mauritania). The Caledonian orogen and Palaeozoic orogenesis. IGCP Project 27 Symposium Morocco, Rabat, p 23

Lécorché JP, Dallmeyer RD, Villeneuve M (1989) Definition of tectonostratigraphic terranes in the Mauritanide, Bassaride, and Rokelide orogens, West Africa. Geol Soc Am Bull 230:131–144 (Special paper)

Mark G, Oliver NHS, Williams PJ, Valenta RK, Crookes RA (2000) The evolution of the Ernest Henry Fe–oxide–(Cu–Au) hydrothermal system. In: Porter TM (ed) Hydrothermal iron oxide copper–gold & related deposits: a global perspective. Australian Mineral Foundation, Adelaide, pp 123–136

Martyn JE, Strickland CD (2004) Stratigraphy, structure and mineralisation of the Akjoujt area, Mauritania. J Afr Earth Sci 38:489–503

Miyano T, Klein C (1989) Phase equilibria in the system K_2O–FeO–MgO–Al_2O_3–SiO_2–H_2O–CO_2 and the stability limit of stilpnomelane in metamorphosed Precambrian iron-formations. Contrib Mineral Petrol 102:478–491

Pertchuk LL, Lavrenteva IV (1983) Experimental investigation of exchange equilibria in the system cordierite–garnet–biotite. In: Saxena SK (ed) Kinetics and Equilibrium in Mineral Reactions. Springer, Berlin Heidelberg New York, pp 199–239

Ponsard JF, Roussel J, Villeneuve M, Lesquer A (1988) The Pan-African orogenic belt of southern Mauritanides and northern Rokelides (southern Senegal and Guinea, West Africa): gravity evidence for a collisional suture. J Afr Earth Sci 7:463–472

Porter TM (2002) Hydrothermal iron oxide copper–gold & related deposits: a global perspective. Porter Geoconsulting Publishing, Linden Park, pp 377

Pouclet A, Guillot P-L, Ba Gatta A (1987) Nouvelles données lithostructurales, pétrographiques, minéralogiques et geochimiques sur le gisement de cuivre d'Akjoujt et son environnement géologique (République Islamique de Mauritanie). J Afr Earth Sci 6:29–43

Ramdohr P (1957) Recherches microscopiques sur les minerais du gisement du Guelb Moghrein (Akjoujt). Bulletin de la Direction Féderale des Mines et de la Géologie, Afrique Occidentale Française, Dakar 20:195–255

Robinson P, Spear FS, Schumacher JC, Laird J, Klein C, Evans BW, Doolan BL (1981) Phase relations of metamorphic amphiboles: natural occurrence and theory. Rev Miner 9B:1–228

Rotherham JF (1997) A metasomatic origin for the iron-oxide Au–Cu Starra orebodies, Eastern Fold Belt, Mount Isa Inlier. Miner Depos 32:205–218

Sillitoe RH (2003) Iron oxide–copper–gold deposits: an Andean view. Miner Depos 38:787–812

Skirrow RG, Walsche JL (2002) Reduced and oxidized Au–Cu–Bi iron oxide deposits of the Tennant Creek Inlier, Australia: an intergrated geologic and chemical model. Econ Geol 97:1167–1202

Sougy J (1969) Grandes lignes structurales de la chaîne des Mauritanides et de son avant-pays (socle précambrien et sa couverture infracambrienne et paléozoique), Afrique de l'Ouest. Bulletin de la Société géologique de France 7:133–149

Strickland CD, Martyn JE (2002) The Guelb Moghrein Fe-oxide copper–gold–cobalt deposit and associated mineral occurrences, Mauritania: A geological introduction. In: Porter TM (eds) Hydrothermal Iron Oxide Copper–Gold & Related Deposits: A Global Perspective. PGC, Adelaide, pp 275–291

Thomas RJ, Fekkak A, Ennih N, Errami E, Loughlin SC, Gresse PG, Chevallier LP, Liégeois J-P (2004) A new lithostratigraphic framework for the Anti-Atlas Orogen, Morocco. J Afr Earth Sci 39:217–226